Inhibition-induced explosive synchronization in multiplex networks

Sarika Jalan,[1,2,3,*] Vasundhara Rathore,[2] Ajay Deep Kachhvah,[1] and Alok Yadav[1]

[1]*Complex Systems Lab, Discipline of Physics, Indian Institute of Technology Indore, Khandwa Road, Simrol, Indore-453552, India*

[2]*Discipline of Biosciences and Biomedical Engineering, Indian Institute of Technology Indore, Khandwa Road, Simrol, Indore-453552, India*

[3]*Laboratory of Systems Medicine of Healthy Aging and Department of Applied Mathematics, Lobachevsky University, Nizhny Novgorod, Russia*

(Received 24 November 2018; revised manuscript received 14 April 2019; published 14 June 2019)

To date, explosive synchronization (ES) in a network is shown to be originated from considering either degree-frequency correlation, frequency-coupling strength correlation, inertia, or adaptively controlled phase oscillators. Here we show that ES is a generic phenomenon and can occur in any network by multiplexing it with an appropriate layer without even considering any prerequisite for the emergence of ES. We devise a technique which leads to the occurrence of ES with hysteresis loop in a network upon its multiplexing with a negatively coupled (or inhibitory) layer. The impact of various structural properties of positively coupled (or excitatory) and inhibitory layers along with the strength of multiplexing in gaining control over the induced ES transition is discussed. Analytical prediction for the spread of phase distribution of each layer is provided, which is in good agreement with the numerical assessment. This investigation is a step forward in highlighting the importance of multiplex framework not only in bringing phenomena which are not possible in an isolated network but also in providing more structural control over the induced phenomena.

DOI: 10.1103/PhysRevE.99.062305

I. INTRODUCTION

Synchronization of networked phase oscillators has proven itself to be an important process in understanding the collective behavior of a variety of real-world complex systems ranging from physical to biological systems [1–8]. Gardeñes *et al.* [9] reported that the transition to synchronization can be an abrupt or first-order type, called explosive synchronization (ES), and can be achieved by setting a correlation between the natural frequencies and respective degrees of networked phase oscillators. Owing to the significance of ES in elucidating various abrupt transitions found in real-world systems, for instance, massive blackouts (cascading failure of the power stations) [10] or epileptic seizure (the abrupt synchronous firing of neurons) [11], chronic pain in the FM brain [12], and bistable Cdc2-cyclin B in embryonic cell cycle [13], ES has received tremendous attention from the network science community [9,14–24]. Experimental evidence of explosive synchronization has also been reported in star network of electronic circuits [25] and mercury beating-heart oscillators [26]. Tanaka *et al.* [27] introduced the occurrence of the first-order (discontinuous) transition resulting from finite inertia in the networked Kuramoto oscillators. Lately, further studies on ES have demonstrated that the microscopic correlation between degree frequency is not the only criteria for the occurrence of ES. For instance, ES is also shown to result from a fraction of adaptively controlled oscillators [28–30], and by assuming a positive correlation between coupling strengths and respective absolute of natural frequencies of networked oscillators [24] in isolated networks. All the investigations reinforce the fact that any suppressing factor, which hampers the growth of the largest synchronized clusters, leads to the abrupt formation of a single giant synchronous component [15].

Lately, the investigations on ES have been extended to multilayered networks by considering a fraction of adaptively controlled Kuramoto oscillators [28], second-order Kuramoto oscillators (with inertia) [31,32], and intertwined multilayer couplings [33,34]. A multiplex network [3,35–43] is a framework of interconnected layers, each with different connectivity explicating different dynamical processes, however, represented by a common set of nodes. It provides a more accurate representation of many real-world networks [44–46]. Further, inclusion of inhibitory nodes have been shown to impart various dynamical [47] and statistical properties [48–50] of underlying network. The inhibitory coupling is known to show multistability [51,52] and suppress synchronization in networked phase oscillators [53,54]. For instance, inhibition is a significant factor in controlling excessive synchronization among neurons, which destroys complex interaction patterns in a brain network and gives rise to neurological disorders like epileptic seizures [55]. It is reported in a recent study [56] that ES transition in a single layer network can be suppressed by making a fraction of oscillators negatively coupled. On the contrary, in the current study, we demonstrate that ES can emerge in a network if the nodes, by some means, remain under the impression of significant inhibition or suppression all the time. We show that ES can be induced in any given network, without employing any precondition giving rise to ES, by multiplexing with a layer with negative connectivity. We, therefore, multiplex a layer (excitatory) of positively coupled nodes to a layer (inhibitory) with negatively coupled nodes to bring in the suppressive effect in the system. We further conjecture that one can find a critical negative coupling

*sarikajalan9@gmail.com

strength which could produce the suppressive effect, through multiplexing, sufficient enough to suppress the formation of the giant cluster in the positively coupled layer leading to ES. Eventually, we prove our conjecture to be true by demonstrating the occurrence of ES in the excitatory layer for a variety of multiplex networks. Further, we discuss how the structural properties of the multiplex network provide us with control over the emergent ES. We also predict analytically the spread of synchronized phases in each layer, which closely follows our numerical assessment.

II. METHODS

In the current work, we investigate how the route to synchronization in a network gets affected in the presence of inhibition, introduced via multiplexing the network with an inhibitory network. To accomplish this, we consider an undirected and unweighted multiplex network comprising M layers, each having N nodes. Here, the dynamics of each node is determined by the most celebrated Kuramoto oscillators [57]. To incorporate inhibition, one layer of the multiplex network is subject to the inhibitory coupling between the nodes. Here, we investigate the impact of inhibition on intralayer synchronization in the multiplexed layers with different sets of choices for network topologies. For the sake of comparison, we will restrict our study to two-layered multiplex networks. Hence the time evolution of Kuramoto oscillators in a duplex network with such a scenario is governed by

$$\dot{\theta}_1^i = \omega_1^i + \lambda_+ \sum_{j=1}^{N} A_1^{ij}\left[\sin\left(\theta_1^j - \theta_1^i\right)\right] + D_x\left[\sin\left(\theta_2^i - \theta_1^i\right)\right],$$
$$\dot{\theta}_2^i = \omega_2^i + \lambda_- \sum_{j=1}^{N} A_2^{ij}\left[\sin\left(\theta_2^j - \theta_2^i\right)\right] + D_x\left[\sin\left(\theta_1^i - \theta_2^i\right)\right], \tag{1}$$

where the subscripts 1 and 2 symbolize two distinct layers. $\theta^i(t)$ and ω^i, where $i = 1, \ldots, N$, denote the initial phase and intrinsic frequency of the ith node, respectively. The parameter D_x represents the interlayer coupling strength between the layers. The positive coupling ($\lambda_+ > 0$) reflects the positive interactions between nodes of the excitatory layer, while negative coupling ($\lambda_- < 0$) accounts for the negative interactions or suppressive behavior in the inhibitory layer. The intralayer connectivity between the nodes following a network topology is encoded in the adjacency matrix A (of dimension $M \times N$) such that $A^{ij} = 1$ (0) if ith and jth nodes are connected (disconnected). Hence the adjacency matrix of the multiplex network can be denoted by the set of intralayer adjacencies, $\{\mathbf{A}_1, \mathbf{A}_2, \ldots, \mathbf{A}_M\}$. For a duplex network, the adjacency matrix is given by

$$\mathcal{M} = \begin{pmatrix} \mathbf{A}_1 & D_x\mathbf{I} \\ D_x\mathbf{I} & \mathbf{A}_2 \end{pmatrix}, \tag{2}$$

where $\mathbf{I}$ is the identity matrix. A schematic representation of a two-layered multiplex network with excitatory (positive) and inhibitory (negative) layers connected via interlayer coupling is given in Fig. 1. To track the degree of coherence or synchronization in the multiplex network, we define the global order

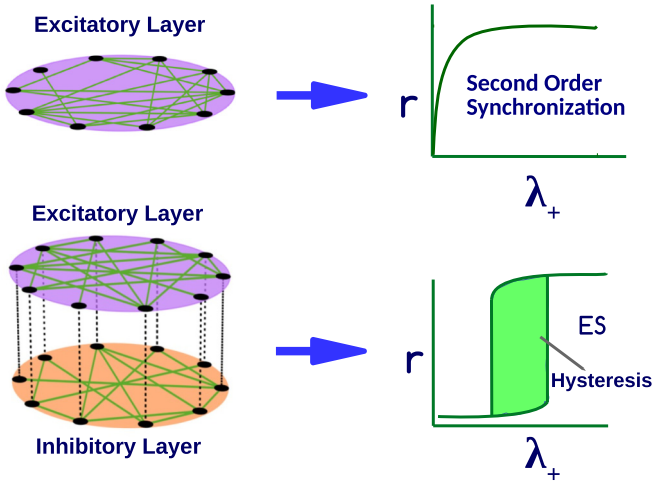

FIG. 1. Schematic diagram for a single layer network where nodes are positively coupled, depicting a smooth second order transition to synchrony (top). Multiplex network in which the same nodes are positively and negatively coupled separately in two different layers, called excitatory and inhibitory, respectively (bottom). Parameter r depicts the degree of coherence as a function of coupling strength λ as defined in Eq. (3). The positively coupled layer shows ES transition with hysteresis upon multiplexing with a negative layer.

parameters r_1 and r_2 for both the layers in terms of average phases ϕ_1 and ϕ_2 as

$$r_1(t)e^{\iota\phi_1} = \frac{1}{N}\sum_{k=1}^{N} e^{\iota\theta_1^k},$$
$$r_2(t)e^{\iota\phi_2} = \frac{1}{N}\sum_{k=1}^{N} e^{\iota\theta_2^k}. \tag{3}$$

Hence $r_1 = 1$ ($r_2 = 1$) represents a completely synchronous state, while $r_1 = 0$ ($r_2 = 0$) implies total incoherence.

Additionally, if T is the total time (long enough) of averaging after discarding initial transients t_r of the system states, the effective frequency $\langle\omega^i\rangle$ of each node in a network is defined as

$$\langle\omega^i\rangle = \frac{1}{T}\int_{t_r}^{t_r+T} \dot{\theta}^i(t)dt. \tag{4}$$

We also define a symmetric matrix encoding the degree of coherence between every pair of linked nodes as [58]

$$r^{ij} = A^{ij}\left|\lim_{T\to\infty}\frac{1}{T}\int_{t_r}^{t_r+T} e^{\iota[\theta^i(t)-\theta^j(t)]}dt\right|, \tag{5}$$

so that $0 \leqslant r^{ij} \leqslant 1$. $r^{ij} = 1$ if a pair (i, j) of linked nodes are completely coherent and $r^{ij} = 0$ if completely incoherent. Hence the local composition of the synchronization patterns in a network can be captured by the fraction of all synchronized links defined as

$$r^{\text{link}} = \frac{1}{2N_c}\sum_i\sum_j r^{ij}, \tag{6}$$

where $2N_c$ is the total number of existing links in a network.

III. RESULTS AND DISCUSSIONS

In this section, we will discuss in detail different numerical results exploring the behavior of the path to synchronization in the excitatory layer when it is multiplexed with an inhibitory layer. To achieve this, we study the synchronization profile of each layer by computing order parameters r_1 and r_2 defined in Eq. (3) as a function of the coupling strength.

To induct inhibition in coupling between all the pairs of nodes in the inhibitory layer, λ_- is fixed to a constant negative value. Further, to track transition to synchronization, the coupling strength λ_+ is varied. First, λ_+ is increased adiabatically starting from $\lambda_+ = 0$ (incoherent state) to $\lambda_+ + n\delta\lambda_+$ corresponding to a synchronous state, in the step of $\delta\lambda_+$. Second, to verify the existence of hysteresis, we adiabatically decrease λ_+ from $\lambda_+ + n\delta\lambda_+$ (synchronous) to $\lambda_+ = 0$ (incoherent) in the step of $\delta\lambda_+$. We name the above two processes as forward and backward transitions, respectively. The order parameters r_1 and r_2 are computed at each step $\delta\lambda_+$ during increment as well as decrement of λ_+. For our simulations, we have taken $\delta\lambda_+ = 10^{-3}$. We integrate the system [Eq. (1)] using the RK4 method with step size $dt = 0.01$ for long enough time (5×10^4 time steps) to arrive at a stationary state after eliminating initial transients. For both the layers, initial values of phases θ^i and natural frequencies ω^i are drawn uniformly randomly in the range $[0, 2\pi)$ and $[-0.5, 0.5]$, respectively. For the sake of comparison and to perform a variety of analysis, we have considered a duplex network comprising a globally connected GC (excitatory) and regular ring (inhibitory) layers each having $N = 50$ nodes with $D_x = 2$, otherwise mentioned elsewhere.

It is known that a monoplex GC layer exhibits second order transition [Fig. 2(a)]. When the GC layer is multiplexed with a positively coupled layer (regular ring network), the second order nature of transition in the GC layer persists with no hysteresis observed in the forward and the backward transitions [Fig. 2(b)]. Next, when the GC layer is multiplexed with a negatively coupled (inhibitory) layer with a fixed λ_-, which is considerably larger than the critical value of λ_+ required for transition of the excitatory layer, strikingly the GC layer (r_1) starts exhibiting ES (first order) transition with associated hysteresis loop in the forward and the backward transitions [Fig. 2(c)]. Moreover, the value of order parameter r_2 for the inhibitory layer remains low ($r_2 < 0.1$), i.e., it does not show global synchronization [see Fig. 2(d)]. This behavior of the inhibitory layer is similar to that of the monoplex one. However, a close examination of the value of r_2 reveals that the inhibitory layer too experiences the ES transition with a hysteresis loop at the same values of forward and backward coupling strength as those of the excitatory layer. However, the jump size is very small as it gets suppressed by the strong inhibition within the layer.

A. Behavior of $\langle\omega^i\rangle$, r, and r^{link}

To have a deeper understanding about the underlying microdynamics taking place in the asynchronous and synchronous states of both the layers, we closely look at the behavior of microscopic properties such as effective frequencies and r^{link} for each layer.

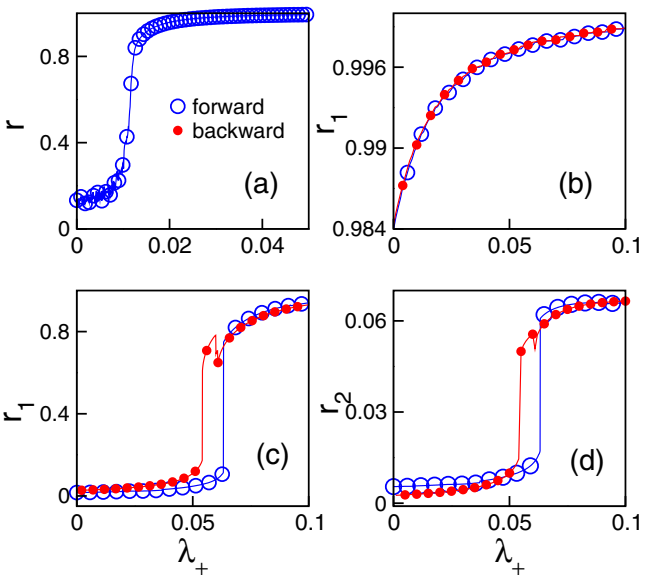

FIG. 2. Order parameters illustrating continuous transition as a function of coupling strength in a positively coupled GC network (a) in its isolation and (b) when it is multiplexed with another positively coupled regular layer. Upon multiplexing with a negatively coupled ($\lambda_- = 2$) regular layer, (c) it exhibits ES transition with a hysteresis (d) while the inhibitory layer shows the first-order jump to another asynchronous state.

Figure 3 illustrates the behavior of order parameters, effective frequencies, and r^{link} of both the layers for different values of inhibitory coupling strength. For a rather weak $\lambda_- = -0.5$, the effective frequencies of the excitatory and inhibitory nodes are spread over a considerable width until a critical value of λ_+ triggers the onset of ES. For any value of λ_+ prior to the ES threshold, the values of r_1^{link} and r_2^{link} range between 0.7–0.85 and 0.8–0.9, respectively, while r_1 and r_2 tend to zero. It indicates that, despite global incoherence, there exists noticeable local clustering of the phases in both the layers. At the brink of transition, nevertheless, the excitatory layer exhibits ES overcoming the inhibitory force as the current locally clustered phases abruptly construct the giant synchronized cluster. At the same time, r_2 gets suppressed, sporting a very short ES jump under the impression of unrelenting intralayer inhibition. For any value of λ_+ post the transition, $r_2^{\text{link}} = 0.99$ and $\langle\omega^i\rangle_2 \simeq 0$, therefore, the inhibitory layer maintains even stronger local clustering of phases. For a bit stronger $\lambda_- = -0.8$, the width of the spread of $\langle\omega^i\rangle_1$ and $\langle\omega^i\rangle_2$ shrinks, and they abruptly converge to mean frequency at the outset of ES at relatively higher λ_+, yielding a more profound ES jump than that for the $\lambda_- = -0.5$ case. For any value of λ_+ prior to the ES threshold, higher $r_1^{\text{link}} = 0.95$ and $r_2^{\text{link}} = 0.96$ imply the existence of more significant local clustering patterns than that for the $\lambda_- = -0.5$ case. A strong enough $\lambda_- = -1$ leads to the oscillation death ($\langle\omega^i\rangle_1 \simeq 0$ and $\langle\omega^i\rangle_2 \simeq 0$) for the excitatory and inhibitory nodes even at the smallest value of λ_+. The values of r_1^{link} and r_2^{link} freeze to 0.99 for any value of λ_+, implying the fact that there exist robust and distinct locally clustered excitatory and inhibitory phases in the respective incoherent regions. Moreover, the strong λ_- gives rise to even steeper r_1 jump and more suppressed

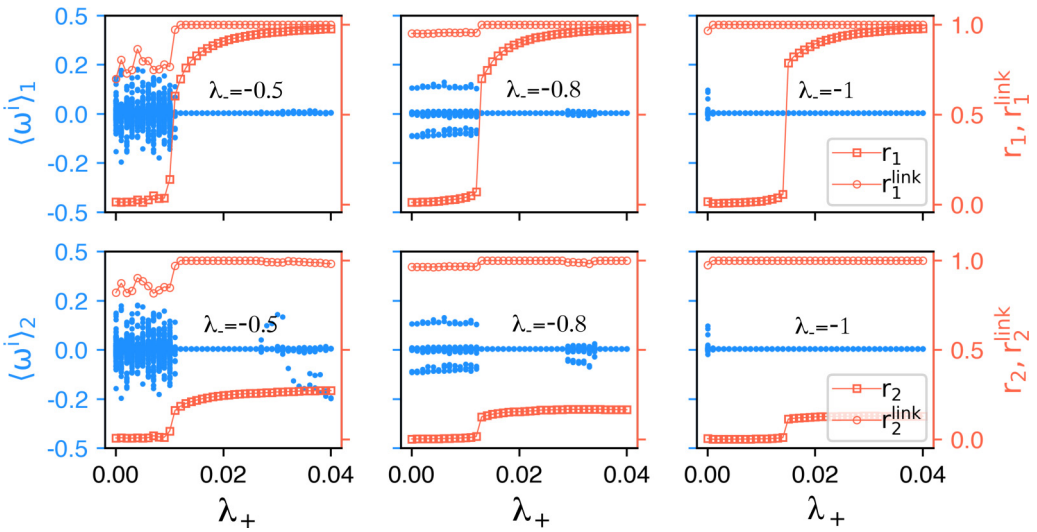

FIG. 3. Effective frequencies, order parameters, and r^{link} of both the excitatory and inhibitory layers as a function of λ_+ for different values of inhibitory coupling strength λ_-. The number of nodes in each layer $N = 200$, $D_x = 2$, and $\langle k_2 \rangle = 10$.

r_2 jump at a further value of λ_+ than that for the case of $\lambda_- = -0.8$.

Hence it is evident that, as λ_- in the inhibitory layer strengthens, it shrinks the width of the spread of effective frequencies of the excitatory and inhibitory nodes to form distinct local clusters of the excitatory and inhibitory phases. For a λ_-, when λ_+ becomes strong enough to overcome the suppressive effect of the inhibitory layer, the distinctly clustered excitatory phases abruptly get synchronized and give rise to ES transition. Nonetheless, λ_+ in the inhibitory layer cannot win over compelling inhibition. Therefore, the robust local clusters of inhibitory phases do not construct a giant global cluster; in turn, ES transition gets suppressed.

Next, we investigate the impact of inhibitory coupling strength on the hysteresis width of the excitatory layer in Fig. 4. The increase in strength of λ_- appears to widen the hysteresis width of forward and backward transitions of the excitatory layer. In Fig. 5, we also study the behavior of order parameter r and r^{link} of the entire multiplex network with increments in λ_+ for different values of λ_-. r, and r^{link} for different strength of λ_- following the behavior of those of the excitatory layer (see Fig. 3), except that the value of r (of multiplex network) for any λ_- drops between 0.5 and 0.65, which is perceptible as it represents the combined coherence of the excitatory and inhibitory layers.

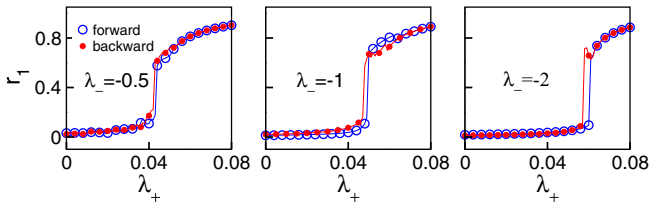

FIG. 4. Order parameter r_1 of the excitatory layer (for $N = 50$ nodes, and $D_x = 2$) in forward and backward transitions, for different values of inhibitory coupling strength, demonstrating hysteresis curves.

B. Evolution and distribution of phases in a layer

To have a far down insight into the behavior of the excitatory and inhibitory layers, we analyze the time evolution and distribution of phases for both the layers of the multiplex network prior and post the outset of transition.

Phase evolution of a layer. We study time series of the phases of the nodes in each layer before and after the onset of ES (see Fig. 6). We find that, after the onset of ES, the phases in the excitatory layer are synchronized, while the phases in the inhibitory layer remain stationary yet do not exhibit global synchrony as the strong inhibition within the layer suppresses it. Before the onset of ES, the inhibitory layer exhibits stationary phases because of the strong intralayer inhibition felt; nevertheless, the excitatory layer also surprisingly exhibits stationary phases, but due to inhibition felt through intralayer links.

Figure 7 depicts the radar representation of phases of the excitatory (GC) and inhibitory (regular) layers at two different times t_1 and t_2 prior and post the transition. Here, the natural frequencies of θ_1 and θ_2 are uniformly selected between zero and 1 instead of -0.5 and 0.5 as considered for Fig. 6 where

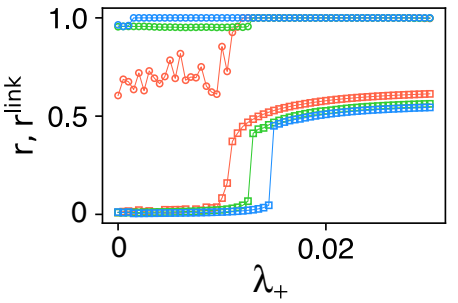

FIG. 5. Order parameter r (square) and r^{link} (circle) of the multiplex network as a function of λ_+ for different values of λ_-. Squares and circles in red, green, and blue colors correspond to $\lambda_- = -0.5$, -0.8, and -1, respectively. The results are included for $N = 200$ nodes in each layer.

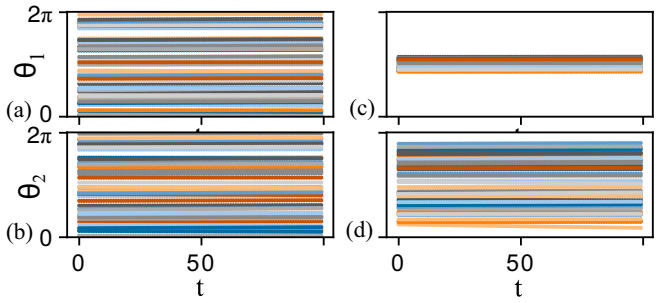

FIG. 6. Time series of the phases of the nodes in the excitatory (θ_1) and inhibitory (θ_2) layers before [(a) and (b)] and after [(c) and (d)] the onset of ES. Time series are obtained for $N = 50$ nodes in each layer interacting under the impression of $\lambda_- = -0.5$ and $D_x = 2$.

phases of both the layers appear stationary with time prior and post the transition. It is evident from Fig. 7 that, for both before and after transition cases, the phases θ_1 (θ_2) rotate with the same frequency and preserve the angular distance with each other and hence their distribution.

Phase distribution $P(\theta)$ of a layer. In Fig. 8, first and third row panels illustrate the binned phases of the excitatory and inhibitory layers, respectively, as a function of coupling strength λ_+ for different values of inhibitory coupling strength. Second and fourth row panels depict distributions of the excitatory θ_1 and inhibitory θ_2 phases, respectively, for a

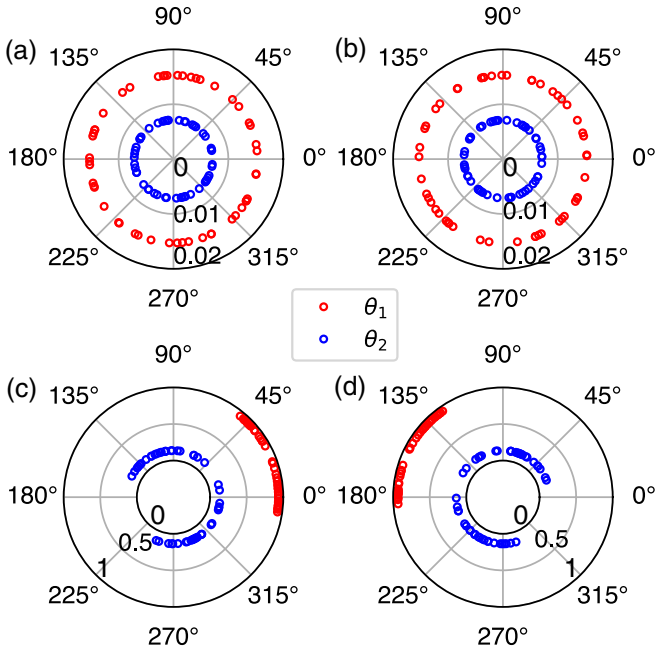

FIG. 7. Radar plots of the excitatory GC (θ_1) and the inhibitory regular ring (θ_2) phases at two different instants $t_1 = 1$ [(a) and (c)] and $t_2 = 500$ [(b) and (d)] before [(a) and (b)] and after [(c) and (d)] the triggering of ES. The radar plots are presented for $D_x = 2$, $\lambda_- = -1$, and $N = 50$ nodes in each layer with natural frequencies uniformly drawn in the range 0 and 1. All θ_1 (θ_2) rotate with constant frequency maintaining the angular distances with each other over time.

value of λ_+ less than ($\lambda_+ < \lambda_c$) and greater than ($\lambda_+ > \lambda_c$) ES threshold λ_c. The top panels for θ_1 make it apparent that, before the onset of ES ($\lambda_+ < \lambda_c$) for different values of λ_-, the excitatory phases are uniformly clustered into uniform bins covering the entire phase range $[0, 2\pi]$, which becomes further apparent from histograms (blue) in corresponding second row panels. Also, after the onset of ES ($\lambda_+ > \lambda_c$) for different values of λ_-, the excitatory phases are nearly synchronized and spread out over a few sequenced bins (top panels). The distribution for $\lambda_+ > \lambda_c$ (orange) in the second row panels further confirms phase synchronization with narrowly distributed bimodal peaks. In similar fashion, for any value of λ_+ in the incoherent region, the inhibitory phases θ_2 are also uniformly distributed in the entire phase range $[0, 2\pi]$ for different values of λ_-, which is also corroborated from distribution ($\lambda_+ < \lambda_c$, blue) in corresponding fourth row panels. However, post the outset of ES ($\lambda_+ > \lambda_c$), phases θ_2 are broadly distributed in bimodal peaks for the lower strength of λ_-. As the strength of λ_- is increased further, phases θ_2 now gradually start following uniform distribution covering the range $[0, 2\pi]$, which is manifested from histograms (orange) in bottom panels.

Further, we analytically demonstrate the existence of two peaks of distributed phases for the excitatory and inhibitory layers [see $P(\theta_1)$ and $P(\theta_2)$ for low λ_- in Fig. 8] after ES transition. We start with rewriting the time evolution of Kuramoto oscillators Eq. (1) in a duplex network in the following composite form:

$$\dot{\theta^i} = \omega^i + \lambda_\pm \sum_{j=1}^{2N} A^{ij} \sin(\theta^j - \theta^i) + (D_x - \lambda_\pm) \sin(\theta^l - \theta^i), \tag{7}$$

where $i = 1, 2, \ldots, 2N$,

$$\lambda_\pm = \begin{cases} \lambda_+, & \text{if } i \leqslant N, \\ \lambda_-, & \text{if } i > N, \end{cases}$$

$$\theta^l = \begin{cases} \theta^{i+N}, & \text{if } i \leqslant N, \\ \theta^{i-N}, & \text{if } i > N. \end{cases}$$

Equation (7) can be expressed in terms of local order parameter $r^i e^{\iota\psi^i} = \frac{1}{(k^i+1)} \sum_{j=1}^{2N} A^{ij} e^{\iota\theta^j}$ for a node i having local average phase ψ^i arising from k^i neighbors as

$$\dot{\theta^i} = \omega^i + \lambda_\pm r^i (k^i + 1) \sin(\psi^i - \theta^i) + (D_x - \lambda_\pm) \sin(\theta^l - \theta^i), \tag{8}$$

which can be simplified further in the following:

$$\dot{\theta^i} = \omega^i + \lambda'_\pm \sin(\psi^i - \theta^i + \alpha_\pm), \tag{9}$$

where parameters $\alpha_\pm$ and $\lambda'_\pm$ are respectively defined as

$$\tan \alpha_\pm = \pm \frac{(D_x - \lambda_\pm)}{\lambda_\pm r^i (k^i + 1)},$$
$$\lambda'^2_\pm = [\lambda_\pm r^i (k^i + 1)]^2 + (D_x - \lambda_\pm)^2. \tag{10}$$

Equations (9) and (10) reveal that the nodes in both the layers have their phases distributed into two peaks at ($\psi^i \pm \alpha_\pm$) with

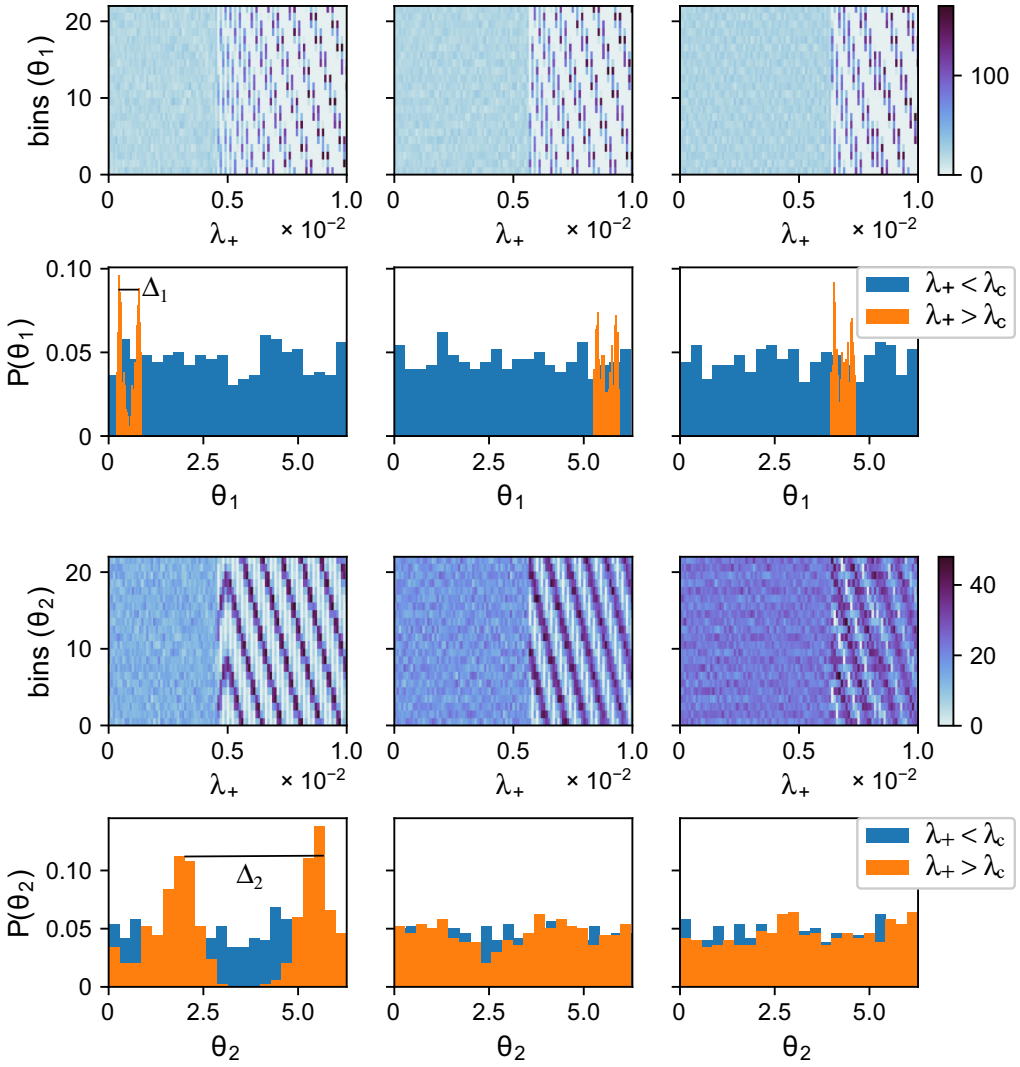

FIG. 8. Binned excitatory θ_1 (top row panels) and inhibitory θ_2 (third row panels) phases with each increase in λ_+, associated with inhibitory coupling strength $\lambda_- = -0.5$ (left panels), -1 (middle panels), and -2 (right panels). Second and bottom row panels depict distributions of the excitatory and inhibitory phases, respectively, before ($\lambda_+ < \lambda_c$) and after ($\lambda_+ > \lambda_c$) the onset of ES. Results are presented for $N = 500$ nodes in each layer and $D_x = 2$. Δ_1 and Δ_2 stand for the gap between peaks for the excitatory and inhibitory layers, respectively.

total separation between the peaks being

$$\Delta = 2\tan^{-1}\frac{(D_x - \lambda_\pm)}{\lambda_\pm r^i(k^i+1)}. \tag{11}$$

Hence the separation Δ depends upon the strength of r_i, D_x, and $\lambda_\pm$. Figure 9 depicts Δ, the separation between two bimodal peaks corresponding to $\lambda_- = -0.5$ for the phases of the excitatory and inhibitory layers as a function of λ_+ [see $P(\theta_1)$ and $P(\theta_2)$ for $\lambda_+ > \lambda_c$ in Fig. 8]. For a λ_+ prior to transition, the excitatory and inhibitory phases do not follow bimodal distribution and instead are uniformly distributed; hence $\Delta_1(\Delta_2) = 0, \pi, \ldots$ as $r_1 \simeq 0$ ($r_2 \simeq 0$). After the transition, nevertheless, separation Δ_1 decreases with each increase in λ_+ as the two peaks get closer, which may eventually merge into a single one when λ_+ approaches D_x, i.e., $D_x \simeq \lambda_+$, while separation Δ_2 starts saturating to some constant value with increase in λ_+. Hence a good agreement between our analytical prediction and numerical estimation manifests the validity of our results. Also, θ^l and ψ^i obey the relation $\tan\theta^l \tan\psi^i = -1$, which yields

$$\theta^l = \psi^i \pm \frac{\pi}{2} + 2n\pi, \quad \forall n = 0, 1, 2, \ldots. \tag{12}$$

This implies that the phase of an excitatory (inhibitory) node and local mean phase of its counterpart in the inhibitory (excitatory) layer maintain a difference of $\pi/2$, i.e., $\theta^l = \psi^i \pm \frac{\pi}{2}$, for $n = 0$.

Theory behind the origin of ES. The employed technique for the emergence of ES works under the constraint that the inhibitory coupling strength must be more significant than the excitatory coupling strength, i.e., $\lambda_- \gg \lambda_+$. Therefore, λ_- is kept fixed to a value much larger than the critical value of λ_+ required for the transition of the excitatory layer so that the excitatory nodes all the time remain under the impression of suppression. Under the effect of this constraint, each node in the inhibitory layer is subject to strong negative interactions from all intralayer neighbors and a single positive interlayer interaction, thereby suppressing global synchronization in the

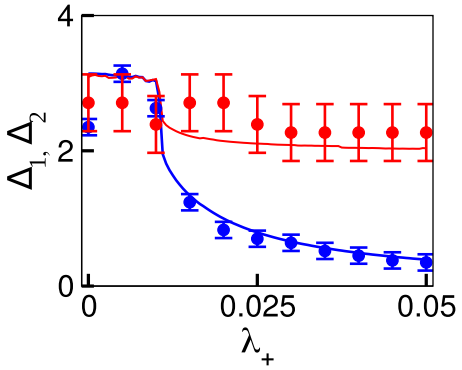

FIG. 9. Separation [Eq. (11)] Δ_1 (blue color) and Δ_2 (red color) between two bimodal peaks in the excitatory, and inhibitory phase distributions, respectively, as a function of λ_+. Line denotes analytical prediction, while filled circle denotes numerical estimations. The results are included for $N = 200$, $D_x = 1$, and $\lambda_- = -0.5$.

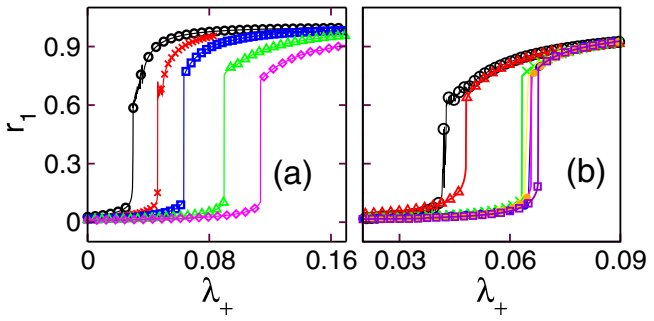

FIG. 10. r_1 as a function of λ_+ for the multiplex network comprised of a positive GC and negative regular networks for different values of (a) interlayer coupling strength $D_x = 1$ (circle), 1.5 (×), 2 (square), 3 (triangle up), and 4 (diamond), and (b) inhibitory coupling strength $\lambda_- = -0.5$ (black circle), -1 (red triangle up), -2 (green ×), -3 (yellow circle), -4 (blue circle), -5 (orange circle), and -8 (violet square).

inhibitory layer. The inhibitory nodes are driven by very strong inhibition to form distinct local clusters of uniformly distributed inhibitory phases leading to oscillation death (see Fig. 8 and bottom panels of Fig. 3). However, each node in the excitatory layer is subject to positive coupling with all its intralayer neighbors and strong negative coupling through the only interlayer inhibitory node. Under the effect of constraint and appropriate multiplexing strength, the compelling suppression from each inhibitory node on its mirror excitatory node impedes coherence in the excitatory layer to some extent until a critical coupling λ_+ at which abrupt ES transition takes place. The excitatory nodes in the incoherent state following the mirror inhibitory nodes also tend to construct distinct local clusters of phases which under the significant inhibition lead to oscillation death (see Fig. 8 and top panels of Fig. 3). Thus appropriate choices of the parameter D_x and λ_- enable us to control the characteristics of emergent ES.

C. Impact of structural properties on ES

Next, we discuss how various structural properties or parameters associated with the multiplex network under consideration affect the occurrence of ES in the excitatory layer.

Impact of D_x on ES. Here, we show that the interlayer coupling strength D_x plays a crucial role in determining the onset of ES, i.e., the critical coupling strength λ_+^c. Figure 10(a) illustrates ES transition in the excitatory GC layer for different values of interlayer coupling strength D_x. An apparent increase in λ_+^c is observed with increment in the interlayer coupling strength. This observation can be attributed to the fact that an increment in D_x leads to a strong impact of inhibition, through multiplexing, on the excitatory nodes from the inhibitory layer. This further hinders or delays the abrupt formation of the giant cluster or suppression of synchrony in the excitatory layer. However, at a sufficiently high coupling strength λ_+^c, all the nodes in the excitatory layer exhibit a sudden jump and formation of the largest synchronized cluster takes place. Thus λ_+^c increases with each increase in D_x. Furthermore, it presents the importance of choosing a multiplex framework where, along with the negative coupling, the interlayer coupling strength also contributes to determining the coupling strength threshold for the ES transition.

Impact of λ_- on ES. Further, we investigate the impact of the strength of inhibitory coupling on ES observed in the excitatory layer. As the magnitude of the inhibitory coupling λ_- in the inhibitory layer is increased, initially both the critical coupling λ_+^c and the abrupt jump size in r_1 increase considerably [Fig. 10(b)]. However, beyond a certain value of the inhibitory coupling, the increments in the value of both λ_+^c and abrupt jump size slow down and start saturating to their respective constant values. Hence the degree of suppression in the excitatory layer increases significantly up to a certain value of the inhibitory coupling strength and beyond which the degree of suppression gradually starts saturating.

Impact of network size N on ES. We carry forward our numerical analysis for the duplex network, with different network sizes. Figure 11 depicts the effect of network size N on ES transition observed in the excitatory GC layer. It is apparent that, with an increase in the size of network, the critical coupling strength decreases as a large number of nodes accelerates contributing to the onset of the ES process.

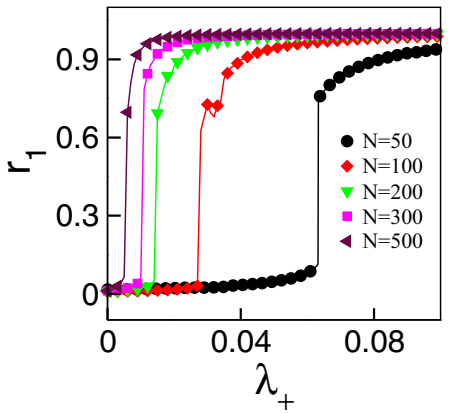

FIG. 11. r_1 as a function of λ_+ for a multiplex network comprised of a positive GC and a negative regular network for different values of the network size.

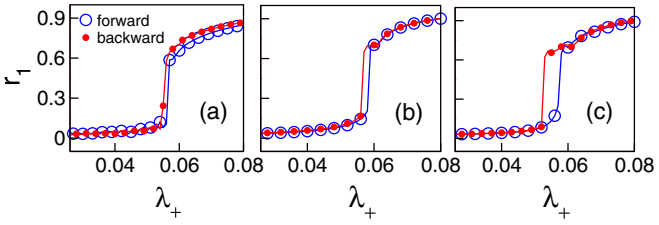

FIG. 12. r_1 as a function of λ_+ when excitatory layer is fixed as GC network and it is multiplexed with different network architectures for the inhibitory layer, (a) GC, (b) ER, and (c) SF. Here $\langle k_1\rangle = \langle k_2\rangle = 10$ and $D_x = 2$.

So far, we have demonstrated that the inhibitory coupling in the regular layer accounts for the emergence of ES in the excitatory GC layer. However, it is important to validate the robustness of the existence of ES induced by the inhibitory coupling for different network architectures of the two layers.

Robustness of ES against network topology of the inhibitory layer. Here we validate the emergence of ES by selecting a different network topology for the inhibitory layer while keeping topology of the excitatory layer fixed to the GC network. The excitatory layer exhibits ES transition to synchrony when the inhibitory layer is tested for GC, ER, and SF topologies (Fig. 12). Hence we emphasize that a positively coupled layer, when multiplexed with a negatively coupled layer of any network topology, gives rise to the ES transition.

Robustness of ES against network topology of the excitatory layer. Here we validate the emergence of ES against different network topologies chosen for the excitatory layer. For the validation of the occurrence of ES, we consider scale-free (SF), random ER, or regular ring networks to represent the excitatory layer. We fix topology of the negative layer to a regular network.

Figure 13(a) depicts that, upon multiplexing, a SF layer with $\langle k_1\rangle = 10$ displays a second order transition, while a rather dense SF layer with $\langle k_1\rangle = 30$ [Fig. 13(b)] does show an ES transition. It is known that a monoplex sparse SF network requires higher coupling strength to get synchronized as compared to a monoplex ER network of the same connectivity, whereas a dense SF network gets synchronized at relatively weak coupling strength. This is the reason a SF layer with $\langle k_1\rangle = 10$ does not show ES; however, a SF layer with $\langle k_1\rangle = 30$ exhibits ES upon being multiplexed with the inhibitory layer with $\lambda_- = -2$.

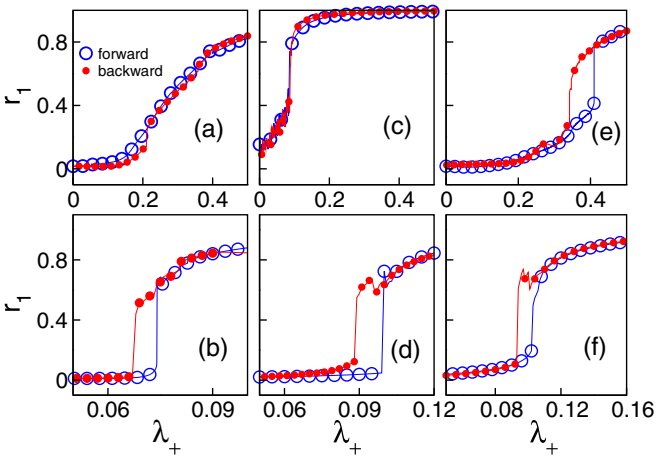

FIG. 13. r_1 as a function of λ_+ for different network architecture of excitatory layer. For all the cases excitatory layer is multiplexed with an inhibitory regular layer, $\langle k_2\rangle = 10$. Panels (a) and (b) correspond to SF layer, (c) and (d) correspond to regular layer, and (e) and (f) correspond to the ER layer for $\langle k_1\rangle = 10$ and $\langle k_1\rangle = 30$, respectively.

Figures 13(c) and 13(d) correspond to the case when the excitatory layer is a regular ring network. In this case, too, a sparse regular network with $\langle k_1\rangle = 10$ leads to a second-order transition, whereas a rather dense regular network with $\langle k_1\rangle = 30$ gives rise to an ES transition. It is known that a monoplex regular network does not synchronize if the node degree is very small. Next, in Fig. 13(e), a random ER layer even with $\langle k_1\rangle = 10$ exhibits an ES transition with hysteresis loop. This can be attributed to the fact that a monoplex ER network gets synchronized at lower coupling strength as compared to a monoplex SF network of the same connectivity. However, a stronger average connectivity $\langle k_1\rangle = 30$ of ER leads to a stronger ES transition [see Fig. 13(f)]. The comparisons carried out against a variety of network topologies reveal that the inhibitory layer can induce an ES transition in the excitatory layer of any network topology provided the fact that it should be capable of achieving the synchronization at a relatively lower coupling strength in the absence of multiplexing.

IV. CONCLUSION

Earlier reported works on ES in the multiplex networks considering adaptive feedback [28] and inertia [31] require that at least one layer in the absence of multiplexing must be exhibiting ES to trigger off ES in all the multiplexed layers. In the present study, strikingly, we have shown that one can induce ES in a layer by multiplexing with an inhibitory layer, hence evading the precondition of having a layer already showing ES without multiplexing. It is revealed that the inclusion of a layer with all negatively coupled links impedes the formation of the largest synchronized cluster in the excitatory layer by propagating suppression via interlayer links, in turn, resulting in the occurrence of ES. It is further shown that such emergence of ES originating from inhibitory coupling remains true for a variety of combinations of network topologies selected for the multiplexed layers. Also, the scheme employed provides us control over the induced ES transition by tuning structural parameters such as average degrees of the layers, inter-, or intralayer coupling strengths. Moreover, we have also proven the validity of our results by showing a good match between theoretical prediction and numerical estimation for separation between the synchronized peaks of the excitatory phases as well as inhibitory phases. Hence, in the present investigation, we have successfully devised a technique to achieve ES by incorporating inhibition through a single layer in a multiplex framework.

The results presented here have applications in understanding synchronization in those systems which, besides having inherent multiplex architecture, have negative coupling between interunits. For example, a two-layered

epithelial-mesenchymal transition process, in which growth involves rapid proliferation of epithelial cells in one layer, while another layer of mesenchymal cells type suppresses proliferation of epithelial cells. In the hair cycle (whole mouse skin), mRNA gene periodic expressions of these two types of cells play a crucial role in the dynamics of growth of hair cells [59]. The positively and negatively coupled layers of gene clusters associated with rapidly growing epithelial cells and inhibitory mesenchymal populations in the hair follicles, respectively, are responsible for the hair cycle dynamical process. In another example, thymic mesenchymal cells derived retinoic acid regulates epithelial cell development in embryonic thymus [60]. Another example of a multiplex network consisting of positive and negative coupling is in ecological systems in which ecological balance exists between facilitation (represents positive interaction) and competition (represents negative interaction) in plant communities. These interactions play a vital role in the structure and organization of plant communities [61]. A similar example is the one of opinion formation in the case of public polling [62]. Those people whose opinion match and they agree share positive interaction, while those who disagree experience negative interactions; a complex interaction between positive and negative coupling determines the outcome.

Hence our investigation about understanding the role of inhibition or suppressive effect on dynamics and its regulation in the multiplex framework can be constructive in learning the underlying dynamics of biological regulatory systems, ecological systems, and formation of prevailing opinion among a group of people.

ACKNOWLEDGMENTS

S.J. acknowledges Govt of India, DST Grant No. EMR/2016/001921, BRNS Grant No. 37(3)/14/11/2018-BRNS/37131, and CSIR Grant No. 25(0293)/18/EMR-II for financial support. S.J. also acknowledges support by the grant of the Ministry of Education and Science of the Russian Federation Agreement No. 075-15-2019-871. V.R. is thankful to Govt of India, DST Grant No. DST/INSPIRE Fellowship/[No. IF180308]. A.D.K. and A.Y. acknowledge Govt of India CSIR Grant No. 25(0293)/18/EMR-II and DST Grant No. EMR/2016/001921 for RA and SRF fellowships, respectively.

[1] S. Boccaletti *et al.*, Phys. Rep. **366**, 1 (2002).
[2] S. Strogatz, *Sync: The Emerging Science of Spontaneous Order* (Hyperion Press, Westport, CT, 2003), Vol. 51, p. 312; W. Kinzel, A. Englert, and I. Kanter, Philos. Trans. R. Soc. A **368**, 379 (2009).
[3] S. Makovkin, A. Kumar, A. Zaikin, S. Jalan, and M. Ivanchenko, Phys. Rev. E **96**, 052214 (2017).
[4] S.-W. Son, B. J. Kim, H. Hong, and H. Jeong, Phys. Rev. Lett. **103**, 228702 (2009).
[5] A. Zeng, S.-W. Son, C. H. Yeung, Y. Fan, and Z. Di, Phys. Rev. E **83**, 045101(R) (2011).
[6] N. Rubido *et al.*, Philos. Trans. R. Soc. A **367**, 3267 (2009).
[7] R. G. Andrzejak *et al.*, Chaos **28**, 091101 (2018).
[8] R. G. Andrzejak, G. Ruzzene, and I. Malvestio, Chaos **27**, 053114 (2017).
[9] J. Gómez-Gardeñes, S. Gómez, A. Arenas, and Y. Moreno, Phys. Rev. Lett. **106**, 128701 (2011).
[10] B. M. Adhikari, C. M. Epstein, and M. Dhamala, Phys. Rev. E **88**, 030701(R) (2013); E. Motter *et al.*, Nat. Phys. **9**, 191 (2013).
[11] R. B. Yaffe *et al.*, Clin. Neurophysiol. **126**, 227 (2015); S. V. Buldyrev *et al.*, Nature (London) **464**, 1025 (2010).
[12] U. Lee, M. Kim, K. Lee, C. M. Kaplan, D. J. Clauw, S. Kim, G. A. Mashour, and R. E. Harris, Nat. Sci. Rep. **8**, 243 (2018).
[13] J. R. Pomerening, E. D. Sontag, and J. E. Ferrell, Jr., Nat. Cell Biol. **5**, 346 (2003).
[14] I. Leyva, I. Sendiña-Nadal, J. A. Almendral, A. Navas, S. Olmi, and S. Boccaletti, Phys. Rev. E **88**, 042808 (2013); I. Leyva *et al.*, Sci. Rep. **3**, 1281 (2013).
[15] S. Boccaletti, J. A. Almendral, S. Guan, I. Leyva, Z. Liu, I. Sendiña-Nadal, Z. Wang, and Y. Zou, Phys. Rep. **660**, 1 (2016).
[16] P. Ji, T. K. DM. Peron, P. J. Menck, F. A. Rodrigues, and J. Kurths, Phys. Rev. Lett. **110**, 218701 (2013); P. Ji, T. K. DM. Peron, F. A. Rodrigues, and J. Kurths, Phys. Rev. E **90**, 062810 (2014).
[17] A. Arenas, A. Díaz-Guilera, J. Kurths, Y. Moreno, and C. Zhou, Phys. Rep. **469**, 93 (2008).
[18] X. Zhang, H. Bi, S. Guan, J. Liu, and Z. Liu, Phys. Rev. E **94**, 012204 (2016).
[19] L. Zhu, L. Tian, and D. Shi, Eur. Phys. J. B **86**, 451 (2013).
[20] A. A. Koronovskii, M. K. Kurovskaya, O. I. Moskalenko, A. Hramov, and S. Boccaletti, Phys. Rev. E **96**, 062312 (2017).
[21] H. Wu, L. Kang, Z. Liu, and M. Dhamala, Sci. Rep. **8**, 15521 (2018).
[22] V. Vlasov, Y. Zou, and T. Pereira, Phys. Rev. E **92**, 012904 (2015).
[23] X. Huang, J. Gao, Y. T. Sun *et al.*, Front. Phys. **11**, 110504 (2016).
[24] X. Zhang, X. Hu, J. Kurths, and Z. Liu, Phys. Rev. E **88**, 010802(R) (2013).
[25] I. Leyva *et al.*, Phys. Rev. Lett. **108**, 168702 (2012).
[26] P. Kumar, D. K. Verma, P. Parmananda, and S. Boccaletti, Phys. Rev. E **91**, 062909 (2015).
[27] H.-A. Tanaka, A. J. Lichtenberg, and S. Oishi, Phys. Rev. Lett. **78**, 2104 (1997).
[28] X. Zhang, S. Boccaletti, S. Guan, and Z. Liu, Phys. Rev. Lett. **114**, 038701 (2015).
[29] M. M. Danziger *et al.*, Chaos **26**, 065307 (2016).
[30] V. Avalos-Gaytán, J. A. Almendral, I. Leyva, F. Battiston, V. Nicosia, V. Latora, and S. Boccaletti, Phys. Rev. E **97**, 042301 (2018).
[31] A. D. Kachhvah and S. Jalan, Europhys. Lett. **119**, 60005 (2017).
[32] A. D. Kachhvah and S. Jalan, New J. Phys. **21**, 015006 (2019); A. D. Kachhvah and A. Sen, arXiv:1407.7823.
[33] S. Jalan, A. Kumar, and I. Leyva, Chaos **29**, 041102 (2019).
[34] V. Nicosia, P. S. Skardal, A. Arenas, and V. Latora, Phys. Rev. Lett. **118**, 138302 (2017).

[35] S. Boccaletti *et al.*, Phys. Rep. **544**, 1 (2017).
[36] F. Radicchi and A. Arenas, Nat. Phys. **9**, 717 (2013).
[37] E. V. Rybalova, T. E. Vadivasova, G. I. Strelkova, V. S. Anishchenko, and A. S. Zakharova, Chaos **29**, 033134 (2019); G. I. Strelkova, T. E. Vadivasova, and V. S. Anishchenko, Reg. Chaotic Dyn. **23**, 948 (2018).
[38] S. Jalan and P. Pradhan, Phys. Rev. E **97**, 042314 (2018).
[39] V. V. Makarov *et al.*, Commun. Nonlin. Sci. Numer. Simulat. **71**, 118 (2019).
[40] D. W. Zhao *et al.*, Sci. Rep. **6**, 24304 (2016).
[41] S. Jalan and A. Singh, Europhys. Lett. **113**, 30002 (2016).
[42] S. Ghosh and S. Jalan, Int. J. Bifurc. Chaos **26**, 1650120 (2016).
[43] S. K. Dwivedi and S. Jalan, Phys. Rev. E **95**, 022309 (2017).
[44] C. Sarkar, A. Yadav, and S. Jalan, Europhys. Lett. **113**, 18007 (2016).
[45] P. Shinde and S. Jalan, Europhys. Lett. **112**, 58001 (2015).
[46] V. V. Makarov, M. O. Zhuravlev, A. E. Runnova, P. Protasov, V. A. Maksimenko, N. S. Frolov, A. N. Pisarchik, and A. E. Hramov, Phys. Rev. E **98**, 062413 (2018).
[47] S. Jalan, S. Ghosh, and B. Patra, Chaos **27**, 101104 (2017).
[48] S. Ghosh, S. K. Dwivedi, M. V. Ivanchenko, and S. Jalan, Europhys. Lett. **115**, 10001 (2016).
[49] S. K. Dwivedi and S. Jalan, Phys. Rev. E **87**, 042714 (2013); **90**, 032803 (2014).
[50] S. Jalan and S. K. Dwivedi, Europhys. Lett. **112**, 48003 (2015).
[51] D. Labavic and H. Meyer-Ortmanns, Chaos **27**, 083103 (2017).
[52] F. Ionita, D. Labavic, M. A. Zaks, and H. Meyer-Ortmanns, Eur. Phys. J. B **86**, 511 (2013).
[53] U. K. Verma, A. Sharma, N. K. Kamal, J. Kurths, and M. D. Shrimali, Sci. Rep. **7**, 7936 (2017).
[54] P. Khanra, P. Kundu, C. Hens, and P. Pal, Phys. Rev. E **98**, 052315 (2018).
[55] M. Chavez, M. Valencia, V. Navarro, V. Latora, and J. Martinerie, Phys. Rev. Lett. **104**, 118701 (2010); K. P. Lamsa *et al.*, Science **315**, 1262 (2007); E. Harvey-Girard *et al.*, J. Neurosci. **30**, 6152 (2010); D. E. Feldman, Neuron **75**, 556 (2012).
[56] X. Zhang, S. Guan, Y. Zou, X. Chen, and Z. Liu, Europhys. Lett. **113**, 28005 (2016).
[57] Y. Kuramoto *Chemical Oscillations, Waves, and Turbulence* (Springer-Verlag, New York, 1984).
[58] J. Gómez-Gardeñes, Y. Moreno, and A. Arenas, Phys. Rev. Lett. **98**, 034101 (2007).
[59] R. Tasseff, A. Bheda-Malge, T. DiColandrea, C. C. Bascom, R. J. Isfort, and R. Gelinas, PLOS Comput. Biol. **11**, 1003914 (2014).
[60] K. M. Sitnik, K. Kotarsky, A. J. White, W. E. Jenkinson, G. Anderson, and W. W. Agace, J. Immunol. **188**, 4801 (2012).
[61] A. Giron, H. Saiz, F. Bacelar, R. Andrade, and J. Gomez-Gardenes, Chaos **26**, 065302 (2016).
[62] S. D. Yi, S. K. Baek, C.-P. Zhu, and B. J. Kim, Phys. Rev. E **87**, 012806 (2013).